Highlights

Late Cenozoic erosion pattern of the eastern margin of the Sichuan Basin: implications for the drainage evolution of the Yangtze River

Ruohong Jiao, Matthew Fox, Rong Yang

- Yangtze River (YR) drainage evolution is studied using linear long profile inversion
- Wu (Upper YR) and Yuan (Middle YR) tributaries were analyzed
- Modeled incision rates are higher in the lower Wu vs. evenly distributed in the Yuan
- Increase in incision rate of the Wu (Upper YR tributary) started in early Miocene
- Increased incision rate was caused by connection between the Upper and Middle Yangtze

Late Cenozoic erosion pattern of the eastern margin of the Sichuan Basin: implications for the drainage evolution of the Yangtze River

Ruohong Jiao[a,*], Matthew Fox[b], Rong Yang[c]

[a]School of Earth and Ocean Sciences, University of Victoria, Victoria, Canada
[b]Department of Earth Sciences, University College London, London, United Kingdom
[c]School of Earth Sciences, Zhejiang University, Hangzhou, China

Abstract

Evolution of the drainage network of the Yangtze River plays an important role in landscape evolution across East Asia during the Cenozoic. The mountains on the eastern margin of the Sichuan Basin form a drainage divide between the tributary rivers of the modern Upper and Middle Yangtze, and the erosion history of these mountains has major implications for the evolution of the Yangtze River. Linear inversion of long profiles of two Yangtze tributaries draining the area allows us to estimate their incision processes, and reveals contrasting erosion patterns between the west and east sides of the mountain belt. Along the Wu River, which drains into the Sichuan Basin, higher incision rates are focused on lower channels near the river's outlet on the Upper Yangtze. In contrast, within the catchment of the Yuan River, which drains into the Jianghan Basin of the Middle Yangtze, the inverted fluvial erosion rate is distributed relatively uniform in space. We calibrate the inferred incision history using previously published cosmogenic ^{10}Be-derived basin-averaged erosion rates, and the results show that the contrasting erosion patterns between the two rivers emerged since the early Miocene (∼21–16 Ma). At this time, the incision rates of the lower Wu River started to increase from ∼0.04 km/Ma towards the Quaternary average at ∼0.07 km/Ma, while the rates of the Yuan River remained low (<0.04 km/Ma). By comparing our results with erosion histories of the eastern Sichuan Basin and Three Gorges, we suggest that during the early Miocene, connection between the Sichuan and Jianghan Basins through the Three Gorges led to additional lowering of the local base level in the Sichuan Basin, which triggered an acceleration in incision rates of the Upper Yangtze tributaries draining into the basin.

Keywords: River incision, Numerical modeling, Sichuan Basin, Yangtze River

*Corresponding author
Email address: `rjiao@uvic.ca` (Ruohong Jiao)

1. Introduction

During the Cenozoic, collision between the Indian and Eurasian Plates and the consequent crustal thickening and uplift of the Tibetan Plateau have created the modern landscape of East Asia (e.g., Harrison et al., 1992; Molnar et al., 1993; Tapponnier et al., 2001; Wang, 2004; Wang et al., 2008), leading to the formation of a long wavelength topographic gradient with a decreasing elevation from the Tibetan Plateau to East China. This dramatic reshaping of the landscape has also led to reorganization of the major river networks surrounding the Tibetan Plateau (e.g., Yan et al., 2012; Tremblay et al., 2015; Gourbet et al., 2020). Several large rivers in East Asia (e.g., Salween, Mekong, and Yangtze) rise and flow southwards on the Tibetan Plateau, but among them only the Yangtze River changes its direction on the margin of the plateau before flowing eastwards into the Sichuan Basin and eventually draining into the East China Sea (Figure 1a). This peculiar pattern of the Yangtze River upstream of the Three Gorges, i.e., the Upper Yangtze (Figure 1b), has inspired a popular hypothesis: prior to the uplift of the Tibetan Plateau, the Upper Yangtze River used to drain southwards into the South China Sea until it was captured by the headwaters of the Middle Yangtze, which also led to the reversal of the flow direction in the Sichuan Basin (Lee and Chao, 1924; Clark et al., 2004; Wang et al., 2013a). For this hypothesis, the timing of the capture and reversal event has been actively debated (e.g., Richardson et al., 2010; Zheng et al., 2013; Zheng, 2015; Sun et al., 2021; Zhang et al., 2021).

To date the birth of a throughgoing Yangtze River between the Tibetan Plateau and the East China Sea, several efforts were made focusing on constraining the age of the Three Gorges, where a drainage divide once existed but now presents deep canyons connecting between the Upper and Middle Yangtze (Li et al., 2001; Richardson et al., 2010; Jiao et al., 2021). However, ages of the fluvial terraces in the gorges (dated by quartz electron spin resonance; Li et al., 2001) and the rapid rock cooling events (constrained by apatite fission-track and U-Th/He thermochronology; Richardson et al., 2010) have led previous studies to suggest disparate timings, i.e., Pleistocene and Eocene, respectively, for the onset of the gorge incision. Moreover, based on geomorphic analysis of the river valleys in the eastern Sichuan Basin, Wang et al. (2013a) inferred that initial incision of the Three Gorges did not necessarily mark the beginning of an east-flowing Upper Yangtze. Because connecting the Upper Yangtze to the drainage systems in East China would significantly change the sediment sources and depositional environment of the basins downstream, other works strove to identify such changes in the sedimentary records in the Lower Yangtze basins in order to date the birth of the modern Yangtze. For example, based on the absence of Cenozoic $^{40}Ar/^{39}Ar$ ages in muscovite and K-feldspar from the late Miocene gravel sediments in the Lower Yangtze, Sun et al. (2021) suggested that the Upper Yangtze was not connected to the drainage systems in East China until after 10 Ma. In contrast, from the same stratigraphic unit based on the temporally invariant U-Pb age patterns of detrital zircons, Zheng et al. (2013) suggested that an east-draining Yangtze River flowing between the Tibetan Plateau and East China had already existed since at least 23 Ma. Such an apparent contradiction between conclusions drawn from sediment provenance analyses highlights the potential bias in detrital geochronology, which could be induced by the process of hydraulic sorting (Reid and Frostick, 1985; Komar, 2007; Garzanti et al., 2008; Malusà et al., 2016) and the variability in the durability and persistence of minerals used as sediment tracers (Mcbride, 1985; Nesbitt et al., 1996). Therefore, without careful quantification of the grain modification effects during weathering, transport, and deposition, the evolution of sediment sources of large rivers inferred by dating single minerals from limited field sites can be problematic (e.g., Vezzoli et al., 2016).

Here, we present a study on the drainage evolution history of the Yangtze River by estimating the incision histories of two major tributaries of the Yangtze, the Wu and Yuan Rivers, on the eastern margin of the Sichuan Basin. Inversion of long profiles of bedrock rivers has been used to infer uplift histories of tectonically active mountain ranges (e.g., Fox et al., 2014; Goren et al., 2014; Ma et al., 2020) or dynamically supported topography (e.g., Roberts and White, 2010; Roberts et al., 2012; Rudge et al., 2015). In the eastern Sichuan Basin, no considerable spatial variability exists in the tectonic deformation nor the climate setting. Rivers in the area flow into the Sichuan Basin of the Upper Yangtze and the Jianghan Basin of the Middle Yangtze, respectively (Figure 1b). Under this setting, a potential contrast in shapes of the river long profiles should mainly reflect different base level histories of the rivers. Our results demonstrate a case that for rivers with temporally stable tectonic uplift rates, their incision histories inverted from long profiles can be used to provide constraints on the reorganization of regional drainage patterns. Compared to previous studies, our investigation to the Yangtze drainage evolution avoids the complication and potential bias associated with long-distance transport and preservation of minerals in provenance analysis, and also does not rely on knowing precisely where the capture events occurred.

2. Geology and geomorphology of the eastern Sichuan Basin

The eastern Sichuan Basin is part of the Yangtze Block, which was amalgamated with the Cathaysia Block during the Neoproterozoic to forge the South China Craton (Zhao, 2015; Cawood et al., 2018; Wang et al., 2018a). The basement rocks in the study area are composed of metamorphosed Precambrian rocks of the Yangtze Block, which are overlain by the Paleozoic and Mesozoic strata (Figure 2). The basement rocks and overlying strata were later deformed as part of an intracontinental thrust system during the Mesozoic (Yan et al., 2003; Chu et al., 2012; Zheng et al., 2019), leading to the formation of the fold and thrust belts which feature as a series of NE-trending chevron or box anticlines and synclines (Zheng et al., 2019; Yan et al., 2003; Li et al., 2012). The Mesozoic deformation had a strong influence on the drainage network on the plateau, presenting as river channels flowing along or traversing the folded strata. Paleozoic and Mesozoic magmatism is widespread in South China (Wang et al., 2013b), but in the study area granitic rocks only occur along the southeast boundary of the catchment of the Yuan River (Figure 2).

The last major deformation phase of the eastern margin of the Sichuan Basin occurred during the early Cenozoic (∼60–40 Ma), as recorded by the cooling paths of the basement rocks inferred from low-temperature thermochronological data (Richardson et al., 2008; Wang et al., 2018b; Qiu et al., 2020). After this period, most of the rocks outcropping on the plateau surface or mountain tops of the region had already been exhumed to near the surface. Due to the southeastward extrusion of the Tibetan Plateau (Tapponnier et al., 1982; Zhang et al., 2004; Royden et al., 2008; Dong et al., 2016), the current movement of the Sichuan Basin can be considered as a clockwise rotation relative to the fixed Eurasia plate, as shown by GPS data (Wang, 2001; Wang and Shen, 2020). However, in the study area on the eastern margin of the basin, impact of the India-Eurasian convergence is insignificant and the strain rate is negligible (Rui and Stamps, 2019).

High topography of the plateau and mountain belt to the east of the Sichuan Basin presents a main drainage divide, separating the tributaries of the Upper and Middle Yangtze River (Figure 1b). The high topography is cut through by the modern Yangtze River in the northeastern corner of the Sichuan Basin in the Three Gorges region, where the river valleys are deeply incised between cliffs and steep mountains (Figure 1b). Atop the mountains surrounding the gorges exist flat or low-relief surfaces, suggesting generally low erosion rates prior to the deep incision of the gorges. These erosion surfaces are distributed throughout the eastern margin of the Sichuan Basin, and continuous towards the Yunnan-Guizhou Plateau and the Tibetan Plateau (Figure 1b). On the southwestern Yunnan-Guizhou Plateau and the eastern margin of the Tibetan Plateau (Figure 1b), the nearly flat or gently tilted surfaces were considered as remnants of a gently undulating relict landscape that formed at low altitude prior to the uplift of the Tibetan Plateau, and therefore their current elevation can be used as a proxy for the surface uplift of the plateau (Schoenbohm et al., 2004; Clark et al., 2006). However, using numerical landscape evolution models Yang et al. (2015) demonstrated that the low-relief surface could also form *in-situ* in response to the loss of catchment area of the rivers, which is a consequence of significant crustal shortening due to indentation of the Indian Plate into the Eurasia. Furthermore, based on modeling of a landscape prior to plateau uplift, Fox et al. (2020) argued that a topography interpolated between the surfaces across the southeastern Tibet required significant variations in channel steepness; this is unexpected in a relict landscape. Nevertheless, unlike the disputed origin of the high-elevation, low-relief surfaces on the margin of the Tibetan Plateau, to the east of the Sichuan Basin where Cenozoic crustal deformation is insignificant (Burchfiel et al., 1995; Tian et al., 2018; Rui and Stamps, 2019), the low-relief surfaces more likely represent an uplifted paleo-erosion surface.

Due to the limited late Cenozoic uplift and crustal deformation, elevations of the eastern margin of the Sichuan Basin (∼800–2000 m) is significantly lower than that of the southwestern Yunnan-Guizhou Plateau (∼1500–3000 m) or the eastern Tibetan Plateau (>3000 m). Accordingly, in contrast to the Upper

Yangtze River and its tributaries on the eastern margin of Tibetan Plateau, e.g., the Jinsha, Min, and Dadu Rivers, the fluvial incision and drainage geometry of rivers on the eastern margin of the Sichuan Basin are not heavily influenced by deformation on active structures (Figure 1b). Based on cosmogenic ^{10}Be measured in quartz in river sands from major tributaries of the Yangtze River, Chappell et al. (2006) estimated catchment-averaged erosion rates at 30–50 m/Ma for tributaries flowing into the Jianghan Basin, including the Yuan River. These rates are lower by an order of magnitude than that of the rivers flowing on the eastern margin of Tibetan Plateau, which yield erosion rates of 300–900 m/Ma. Huang et al. (2013) expanded the previous data set and found that the erosion rate of the Wu River (10–30 m/Ma), despite flowing into the Sichuan Basin, is similar to that of the Yangtze tributaries to the east of the Three Gorges.

3. Methods

3.1. Inversion of river incision history from long profiles

The uplift history of bedrock river channels relative to the base level can be retrieved from the long profile of a river using a linear inversion scheme (Pritchard et al., 2009; Goren et al., 2014; Fox et al., 2014; Rudge et al., 2015). In order to estimate the evolution of the Wu and Yuan Rivers, we invert the long profiles of the two rivers using the method of Goren et al. (2014). The fluvial erosion rate at a point on a bedrock river channel can be predicted using the stream-power model (Howard and Kerby, 1983; Whipple and Tucker, 1999)

$$E(t,x) = KA(x)^m \left(\frac{\partial z(t,x)}{\partial x}\right)^n , \tag{1}$$

in which E is erosion rate, t is time, x is position of a point on the long profile, i.e., distance from the point to the river outlet ($x = 0$), z is elevation, K is a parameter representing the erosional efficiency of the river, A is upstream drainage area, and m and n are positive exponents. To the west of the Sichuan Basin, Ma et al. (2020) were able to fit a linear relationship between the basin-averaged erosion rates and the channel steepness. Without further constraints on the spatial variation in erosion rate in the study area, we adopt the same assumption and assume a linear relationship between the fluvial erosion rate and local channel slope, i.e., $n = 1$. Under this assumption and that the rock uplift rate is invariant in space, the elevation change through time can be predicted as the difference between uplift and erosion, as

$$\frac{\partial z(t,x)}{\partial t} = u(t) - KA(x)^m \frac{\partial z(t,x)}{\partial x} , \tag{2}$$

in which u is rock uplift rate. Combining Equations 1 and 2, one can derive that the upstream migration rate of a knickpoint (i.e., a steepned section of the river) is KA^m (Rosenbloom and Anderson, 1994). Therefore, the time required for a knickpoint to transfer from the outlet to distance x on the river long profile is

$$\tau(x) = \int_0^x \frac{\mathrm{d}x'}{KA(x')^m} , \tag{3}$$

in which x' is an integration parameter. Based on Equations 2 and 3, Royden and Perron (2013) and Goren et al. (2014) showed that the elevation of river channel can be solved as

$$z(t, x) = \int_{t-\tau(x)}^{t} u(t')\,\mathrm{d}t' , \tag{4}$$

in which t is negative and indicates time in the past, and t' is a integration parameter. In Equation 4, $\tau(x)$ is dependent on the erosional efficiency parameter, K. One can factor out K from Equation 4 by introducing three K-dependent variables,

$$\chi = A_0^m K\tau , \tag{5}$$

$$u^* = \frac{u}{KA_0^m} , \tag{6}$$

and

$$t^* = KA_0^m t , \tag{7}$$

where A_0 is an arbitrary value to scale the drainage area, and χ is a lengthscale (Perron and Royden, 2013). After transformation, the present-day elevation of the river profile, i.e., when $t^* = 0$, becomes

$$z(0, x) = \int_{-\chi(x)}^{0} u^*(t^{*\prime})\,\mathrm{d}t' . \tag{8}$$

In order to solve u^*, we follow the method shown in Goren et al. (2014) and Fox et al. (2014) and discretize the uplift history into blocks of Δt^* "intervals". Following this discretization, Equation 8 can be written as a summation of u^* values multiplied by Δt^* values. This can be written as a vector-vector product and a complete dataset of elevation values can be written in matrix form,

$$\boldsymbol{z} = \boldsymbol{G}\boldsymbol{u^*} , \tag{9}$$

in which vector $\boldsymbol{z}$ contains the elevations of all points, $\boldsymbol{u^*}$ is a vector of K-scaled uplift rate, and $\boldsymbol{G}$ is a forward model operator with size of $M \times N$; M and N are the number of elevation points and the number of time intervals, respectively. The summation of all elements in each row of $\boldsymbol{G}$ is equal to the χ value of the point. This expression allows us to calculate elevations along the channel for any $\boldsymbol{u^*}$ history. It also allows us to solve the inverse problem and infer a $\boldsymbol{u^*}$ history from the topographic data and forward model. Here, we solve for a $\boldsymbol{u^*}$ history that is smooth in time. To do this, we seek a solution that minimizes the difference between predicted and observed elevations and the roughness of the history, scaled by a damping factor, λ. Therefore, we minimize

$$\|\boldsymbol{z} - \boldsymbol{G}\boldsymbol{u}^*\|^2 + \lambda^2 \sum \left(\frac{u_i^* - u_{i+1}^*}{t_i^* - t_{i+1}^*} \right)^2 . \tag{10}$$

We solve for non-negative values of $\boldsymbol{u}^*$ using a limited memory Broyden-Fletcher-Goldfarb-Shanno (L-BFGS) algorithm, which has been successfully used for a similar problem (Rudge et al., 2015). After solving $\boldsymbol{u}^*$, uplift rate and time can be calculated using Equations 6 and 7 for a given K. The estimated relative uplift rate u is equivalent to the incision rate at the outlet.

To recover the pre-incision topography of the river channels, we can predict the paleo-elevation of a pixel on the long profile at a time in the past using a general form of Equation 8,

$$z(t^*, x) = \int_{t^* - \chi(x)}^{t^*} u^*(t^{*\prime})\,\mathrm{d}t' . \tag{11}$$

If we assume that the river long profiles were in a steady state, in which fluvial erosion was in equilibrium with the uplift rate, this expression reduces to $z(x) = \chi(x)u^*$.

To prepare the data of the Wu and Yuan Rivers for the inverse problem, we extract the elevation data from the 3 arc-second resolution, hydrologically conditioned SRTM digital elevation model (HydroSHEDS; Lehner et al., 2008). The data is reprojected at 90 m resolution in the Universal Transverse Mercator system. The long profiles of the two rivers are extracted from the reprojected digital elevation model (DEM), where only pixels with upstream drainage area $>10^6$ m^2 are considered as river channels. χ values of the rivers are calculated using A_0=10^6 m^2. The value of the exponent m is optimized by reducing the scatter of the χ-elevation plots (Figure 3), following Goren et al. (2014). For the efficiency of the computation, we exclude topographic data of short tributary branches and only use data of channels that rise onto the erosion surfaces for the inversion. We test different values for the number of time intervals (4–10) and the damping factor, λ (10^6–10^9).

3.2. Constraining the erosion efficiency parameter

Previous studies in many rivers have observed a scaling between the local channel slope and the upstream drainage area (Hack, 1957; Flint, 1974; Howard and Kerby, 1983), consistent with the stream-power model of fluvial erosion. According to Equation 1, the fluvial erosion rate on the current landscape can be predicted as

$$E_0 = KA^m S^n , \tag{12}$$

in which S is the local channel slope ($\mathrm{d}z\,/\,\mathrm{d}x$). The function can be rewritten as

$$E_0 = K\left(\frac{S}{A^{-m/n}}\right)^n = K(k_{sn})^n\,, \tag{13}$$

in which k_{sn} is a normalized channel steepness index. Such a correlation between erosion rate and steepness index provides a means to estimate the mean erosion efficiency, K. Chappell et al. (2006) and Huang et al. (2013) estimated the basin-averaged erosion rates of the trunk stream and main tributaries of the Yangtze River using cosmogenic ^{10}Be concentration in quartz from river sands and sediment yield data from gauging stations. Their results show that for the tributaries to the eastern Sichuan Basin and Lower Yangtze, the ^{10}Be-derived rates are <100 m/Ma and thus represent an average over the past >10 ka (von Blanckenburg, 2005). The analyses of modern sands and Holocene sediments from the Yangtze delta yield consistent results, confirming that the ^{10}Be-derived erosion rates of large basins are reliable estimates for the ka-scale average and unlikely biased by recent mass wasting events (Niemi et al., 2005; Yanites et al., 2009). Therefore, in this paper we use the ^{10}Be-derived erosion rates (Huang et al., 2013) and the mean channel steepness indices of the Wu and Yuan Rivers to estimate the mean erosion efficiency of the rocks in the catchments of the two rivers.

3.3. Mapping of the erosion surface

The uplift rates predicted from long profiles of the Wu and Yuan Rivers represent the elevation changes of the channels relative to their base levels in the Sichuan and Jianghan Basin, respectively. In order to compare the incision magnitudes of the two rivers, we choose the low-relief surfaces across the catchments as a reference. For mapping low-relief erosion surfaces, Haider et al. (2015) demonstrated an efficient method based solely on a DEM. The approach is a fuzzy-logic method, in which the membership functions are based on four critical parameters, i.e., slope, curvature, terrain ruggedness index, and the relative height. As our analysis aims to determine a series of erosion surfaces as a reference level rather than an exhaustive map of the surfaces, we choose to use a definitive description of the erosion surfaces based on the same topographic parameters utilized by Haider et al. (2015). Thus, using a 90 m resolution DEM, we determine the erosion surfaces as areas with surface slope <10°, curvature <0.001 m^{-1}, terrain ruggedness index <50 m, and relative height between 100 and 600 m. The terrain ruggedness index (Riley et al., 1999) is calculated as

$$TRI_{i,j} = \sqrt{\sum_{p=-1}^{1}\sum_{q=-1}^{1}(z_{i,j} - z_{i+p,j+q})^2}\,, \tag{14}$$

in which $z_{i,j}$ and $z_{i+p,j+q}$ are the elevations of a central pixel and one of its 8 neighboring pixels, respectively. The relative height is the elevation difference between a pixel and the nearby main branches of the river network, which we define as the channels with >50 km^2 upstream drainage area. In the Results section, we exclude the small patches and only retain the erosion surfaces with areas >10 km^2.

4. Results

4.1. Channel steepness index

The value of the drainage area exponent, m, is constrained at ~0.5 (Figure 3c), for the fluvial erosion model and channel steepness index calculation. This value is typical in geomorphic analysis, and was used for simulating the landscape of the southeastern Tibetan Plateau (Whipple et al., 2017). The calculated χ-elevation profiles of the Wu and Yuan Rivers yield a reasonable consistency, showing a dominant trend for the majority of the channels albeit lesser scattering of points representing smaller tributary channels (Figure 3).

The calculated channel steepness indices are, of the first order, uniformly distributed across the study area (Figure 4). This general uniformity in channel steepness confirms that no significant spatial heterogeneity in tectonic (e.g., uplift or seismicity), climate (e.g., precipitation rate), and rock erodibility parameters exists within the two catchments to cause considerable variability in erosion rates. For both rivers, low k_{sn} values (<50) constitute ~45 % of the analyzed channel pixels, mainly distributed along the low-gradient main channels, as well as on the low-relief erosion surfaces. The consistently low k_{sn} values on the low-relief surfaces indicate that these surfaces were associated with a former base level under a constant uplift rate (Whipple et al., 2017). High k_{sn} values (>50) are located along steeper tributaries, particularly near the drainage divides or immediately below the erosion surfaces. Due to noises in the DEM, the k_{sn} results include some (<1%) abnormally high values (>1000), but they do not have a considerable impact on our estimates of the river incision history. Specifically, the mean k_{sn} for the Wu and Yuan Rivers are 115.2 and 96.5, respectively, whereas the values would be 99.2 and 90.7 if the >1000 values were excluded from calculation. Eventually, whether the outlier k_{sn} values are included in the calculation or not, the constrained erosion efficiency parameters will be on the same order of magnitude, leading to <0.01 mm/yr and <2 Ma differences in the estimates of the incision rates at the river outlets and the onset time of the accelerated base level fall, respectively. For results presented in this paper, we include all k_{sn} values in the calculation.

4.2. Erosion efficiency parameter

In general, the ^{10}Be concentrations from the Upper Yangtze tributaries on the eastern Tibetan Plateau are lower than that from the tributaries of the Middle and Lower Yangtze (Huang et al., 2013), suggesting a first-order control of tectonics on the erosion rates. After calibration of the ^{10}Be production rate, three estimates of the the basin-averaged erosion rates of the Wu and Yuan Rivers yielded at ~10–30 mm/yr, which were lower by an order of magnitude than that of rivers draining the eastern margin of the Tibetan Plateau

(>250 m/Ma) (Huang et al., 2013); this contrast reflects the divergent tectonic settings between the western and eastern margins of the Sichuan Basin. To determine the erosion efficiency parameter, K, we use the estimated erosion rates of 28.7 m/Ma and 31.5 m/Ma for Wu and Yuan River, respectively, as the other lower rate (11.3 m/Ma) estimated from Wu River is much less consistent with erosion rate estimates from other tributaries of the Yangtze River. Using Equation 13, we determine $K = 3.42\times10^{-7}$ yr^{-1} and $K = 4.63\times10^{-7}$ yr^{-1} for the Wu and Yuan Rivers, respectively. To compare the incision histories between the two rivers, we use a mean value of $K = 4.03\times10^{-7}$ yr^{-1}, but note that the potential variation in K shown here could account for the <0.01 mm/yr and <2 Ma difference in the calibrated incision rates and acceleration time of the base level fall, respectively.

4.3. Calibrated incision history

Figure 5 shows the inverted incision rates of the two rivers at their respective outlets, which are calibrated using the erosion efficiency parameter determined above. As one can expect, models with more time intervals or lower damping factors show higher magnitudes of oscillations in incision rates. The results suggest that the long profiles of the two rivers could record the incision histories over the past ∼40 Ma, but inverted rates are unstable for time intervals prior to ∼30 Ma, especially when lower damping factors are used (Figures 5b and 5d). After ∼30 Ma, the solutions are generally consistent between models using different time intervals. For the Wu River, the modeling results suggest an increase in the incision rates starting at ∼21–16 Ma, which is marked as an abrupt change in gradient on the modeled long profile (Figure 6a). In contrast, the models of the Yuan River suggest no significant change in the incision rates, with the temporal variation of the rates almost within ∼0.01 mm/yr (Figure 5c); therefore, the modeled long profile of the Yuan River is close to the shape produced by a constant uplift rate (Figure 6b).

4.4. Erosion surfaces

Throughout the catchment area of the Wu and Yuan Rivers, we have mapped a total of 164,779 low-relief surfaces with a combined area of 2.6×10^4 km^2, including 3,395 surfaces with areas >1 km^2 (total area 1.7×10^4 km^2) and 549 surfaces >10 km^2 (total area 1.0×10^4 km^2). In order to exclude smaller low-relief surfaces that may form due to processes other than regional erosion (e.g., fluvial aggradation, landsliding, and agriculture), we only keep surfaces with areas >1 km^2 for analysis (Figure 4a). Elevations of the remaining erosion surfaces range mostly between ∼150 m and >2500 m, and generally increase from the northeast to the southwest. Frequency distribution of elevation of the mapped low-relief surfaces shows at least two peaks (Figure 4b), consistent with previous inference that the erosion surfaces formed at different ages (Liu et al., 2019; Lv et al., 2020). The most extensive surfaces occur in the high reaches of the Wu River in the south of the catchment, and also expand eastwards across the drainage divide into the Yuan River. These surfaces are distributed between ~650 m and 1700 m, mostly perched at >1000 m elevations. In this area, the large areas and similar elevations across narrow valleys of the low-relief surfaces suggest that their formation was associated with a regional base level. Therefore, we use these surfaces as a reference level to estimate the incision magnitudes of the two rivers.

5. Discussion

5.1. Contrasting incision patterns between the Wu and Yuan Rivers

We estimate the magnitudes of incision of the two rivers during the model period based on the elevations of the reference erosion surfaces (within the boxed area in Figure 4), which is assumed to represent a fossil steady-state landscape prior to the accelerated incision of the Wu River. By extrapolating this landscape down the river profile (Figure 6), we are able to calculate the total elevation changes for the downstream pixels since these surfaces were abandoned. Note that as we assume the elevations of the erosion surfaces have remained stable, the results are relative but useful for comparing the incision patterns between the two rivers.

Our estimates suggest that below the extrapolated steady-state surfaces, substantial downcutting (>150 m) occurred along the downstream channels of the Wu River, whereas along the Yuan River elevation changes have been much less significant (<50 m)(Figure 6). In the catchment of Wu River, deep incision has been focused along the main channels near the river's outlet on the margin of the Sichuan Basin. In contrast, incision is distributed much more uniformly in space within the catchment of the Yuan River, suggesting that long profiles of the river have been in general equilibrium with rock uplift or base-level lowering rates over the model period. As prior to ~21 Ma the modeled incision rates of both the Wu and Yuan Rivers were relatively constant or slightly decreased (Figure 5), the contrasting incision patterns between the two rivers have likely only emerged since ~21–16 Ma, when the incision rate of the Wu River increased while the rate of the Yuan River remained unchanged. There has been no observation showing differential tectonic deformation between the catchments of the two rivers, nor local climate or bedrock lithology changes during the late Cenozoic, so the increase in the incision rate of the Wu River must be a signal propagated upstream from the Sichuan Basin. This suggests an acceleration in the surface lowering rate of the Sichuan Basin since ~21–16 Ma, which will be further tested below.

5.2. Cause for the accelerated incision rate of the Wu River

We suspect that the accelerated incision rate of the Wu River was driven by continuous removal of the sedimentary cover in the Sichuan Basin, which increased the lowering rate of the river's base level, rather than different tectonic uplift/subsidence rates across the eastern boundary of the basin. We test this hypothesis based on the cooling history of rocks from the eastern Sichuan Basin. Tectonic uplift of mountains on the eastern margin relative to the Sichuan Basin would increase exhumation and erosion of the mountain belts, while rocks in the basin would experience reheating (if sediments from erosion accumulated in the basin) or relatively stable thermal history (if sediments bypassed). Conversely, if the surface of the basin was eroded, rocks in the basin would be continuously cooled as the overlying layers were removed.

Low-temperature thermochronology is widely used in geological and geomorphic studies for estimating the rock cooling history. We modeled the thermal history of the eastern Sichuan Basin using apatite fission-track and (U-Th)/He data from a Jurassic sandstone sample (Y31 in Shi et al., 2016) near the main stream of the Yangtze River (Figure 1b). Apatite fission-track and (U-Th)/He thermochronology are both radiometric dating methods, and combined modeling (e.g., Ketcham, 2005; Gallagher, 2012) of the data (i.e., fission-track grain ages, track length distribution, (U-Th)/He grain ages, grain sizes, etc.) can provide estimates on the cooling history of rocks in the temperature range between $\sim$125 and 50°(Gleadow and Duddy, 1981; Farley, 2000). Our inverse modeling of the data is carried out using a transdimensional Markov Chain Monte Carlo method (Gallagher, 2012), and a total of 200,000 time-temperature paths are sampled with the first 50% discarded as the burn-in. The ensemble of post-burn-in models is appraised to infer the probability density function of the time-temperature points (Figure 7a).

Predictions of the weighted mean model from the post-burn-in ensemble yield reasonable fit to the observed data (Figures 7b and c). The thermal history model suggests a monotonic cooling of the rock sample from $\sim$70 °C at $\sim$40 Ma to the surface at the present day (Figure 7). The model shows that since $\sim$20 Ma, the sample has been cooled to temperatures $<$50°and no subsequent reheating to this temperature has been recorded. Using the mean geothermal gradient of the basin (22.5°C/km; Xu et al., 2011) and a surface temperature of $\sim$15°C, a simple calculation suggests a total exhumation of $\sim$2.4 km over the last $\sim$40 Ma. Using an erosion efficiency parameter of $K = 4.03\times10^{-7}$ yr^{-1} and a damping factor of $\lambda = 10^{7.5}$, our river profile inversion predicts an incision rate between 0.04 and 0.075 mm/yr and a total base level drop of $\sim$2.4 km over the past $\sim$40 Ma (Figure 5a). Therefore, the consistency between the thermal history and river incision models supports that the base-level change of the Wu River was mostly due to the surface denudation in the Sichuan Basin. This is also consistent with the absence of Neogene and Quaternary sediments in the eastern Sichuan Basin (Figure 2) and the scarcity of seismic activity on the structures bounding the eastern margin of the basin (Figure 1b). Our river incision model also indicates a minor increase in the rock exhumation rate after $\sim$10 Ma, but this change would have occurred at near-surface temperatures ($<$30°C) and is negligible on the thermal history model.

5.3. Drainage reorganization in the Sichuan Basin

Based on the apatite thermochronological data from surface and borehole samples, Richardson et al. (2008) revealed that the Sichuan Basin has experienced widespread denudation since $\sim$40 Ma, which has removed $\sim$1–4 km sedimentary covering rocks; the timing and magnitude of this denudation event are also shown by our thermal history modeling result (Figure 7). Richardson et al. (2008) suggested a causal link between the post-40 Ma denudation of the Sichuan Basin and the Cenozoic drainage reorganization in the Sichuan Basin, during which the Upper Yangtze drainage systems in the basin that flowed to the southwest were captured by the Middle Yangtze and started flowing eastwards (Clark et al., 2004). Although we agree that such a transition would lead to a rapid lowering of base level and thus widespread denudation of the Sichuan Basin, a large, integrated pre-Oligocene Yangtze River is not supported by the late Eocene ($\sim$36.5 Ma) evaporite and lacustrine deposits in the downstream Jianghan Basin (Zheng et al., 2011, 2013). Moreover, differential exhumation of rocks across some listric reverse faults in the eastern basin suggests that the Eocene–Oligocene denudation in the eastern basin was controlled, at least partially, by shortening structures (Tian et al., 2018).

Based on detrital zircon U-Pb ages from the Miocene strata in Nanjing (Lower Yangtze) in East China, Zheng et al. (2013) suggested that the Upper Yangtze material had started to appear in the Lower Yangtze basin since the early Miocene ($\sim$23 Ma). This inference was challenged by Sun et al. (2021), who analyzed the same Miocene strata ($\sim$23–10 Ma) but found that young ($<$60 Ma) muscovite and K-feldspar ^{40}Ar/^{39}Ar ages, which are characteristic of the rapidly exhuming eastern Tibetan Plateau, are missing from the sedimentary records. Regardless of the potential bias in detrital geochronology (Malusà et al., 2016), Sun et al. (2021)'s observation can be alternatively explained as that during the early Miocene, rocks with young cooling ages had not been exposed on the surface of the eastern Tibetan Plateau. Furthermore, apart from rivers draining the eastern Tibetan Plateau, other Upper Yangtze tributaries in the Sichuan Basin (e.g., the Jialing River) do not supply sediments with young cooling ages. Therefore, Sun et al. (2021)'s data do not rule out an early Miocene connection between the Sichuan Basin and Middle Yangtze, if at that time rivers on the Tibetan Plateau were still flowing southwards (Kong et al., 2009, 2012; Su et al., 2019).

Based on inversion of the long profiles of three small tributaries and thermochronological data in the Three Gorges area, Jiao et al. (2021) suggested a Miocene onset of the gorge downcutting, but did not conclude whether the accelerated incision rate was triggered by connection between the Upper and Middle Yangtze or tectonic uplift of the area. Here, by revealing the contrasting incision patterns between the Wu and Yuan Rivers, we suggest that connection between the Upper and Middle Yangtze through the Three Gorges, which occurred in response to the uplift of the eastern Tibetan Plateau (Clark et al., 2004), led to lowering of the local base level in the Sichuan Basin. This adjustment of the drainage system increased the incision rates of the Yangtze tributaries not only in the Three Gorges area but also around the Sichuan Basin, including the Wu River.

6. Conclusions

Inversion of long profiles of the Wu and Yuan Rivers reveals contrasting incision patterns of the two Yangtze River tributaries that drain the mountain belts on the eastern margin of the Sichuan Basin. Our models assume negligible spatial variation in the uplift rates within area of the river catchments. The modeling results suggest that along the Wu River which drains into the Sichuan Basin of the Upper Yangtze, channels near the river's outlet to the Yangtze River have been preferentially incised, whereas lower erosion rates occur in smaller channels upstream. In contrast, within the catchment area of the Yuan River which drains to the Jianghan Basin of the Middle Yangtze, the modeled incision rates are distributed nearly uniformly in space. By calibrating the incision models in the geological time scale using the cosmogenic ^{10}Be-derived, basin-averaged erosion rates, we show that the contrasting incision patterns began to emerge during the early Miocene ($\sim$21–16 Ma) when incision rates of the Wu River started to increase. From the early Miocene to the Quaternary, the incision rate at the outlet of the Wu River has increased from $\sim$0.04 km/Ma to $\sim$0.07 km/Ma, while the incision of the Yuan Jiang has remained slow ($<$0.04 km/Ma). Our findings support the hypothesis that the drainage system in the Sichuan Basin was reorganized during the early Miocene. During this time, after the Three Gorges being cut through, the southwest-flowing segment of the Yangtze River in the Sichuan Basin was captured by the Middle Yangtze and started flowing eastwards. Connection between the Sichuan and Jianghan Basin would have lowered the local base level of the former, which in turn would not only accelerate the widespread denudation of the basin fill but also increase the incision rates of the Upper Yangtze tributaries draining into the basin.

Acknowledgment

Topographic data used in this study is available from www.hydrosheds.org. TopoToolBox 2 (Schwanghart and Scherler, 2014) was used for processing topographic data. Figure 1 was produced using Generic Mapping Tools (Wessel et al., 2013). A MATLAB implementation of the L-BFGS algorithm (mathworks.com/-matlabcentral/fileexchange/23245-fminlbfgs-fast-limited-memory-optimizer) was used for solving the nonnegative least squares problem. Jiao was supported by the Natural Sciences and Engineering Research Council of Canada (RGPIN-2019-04405). Fox was supported by the Natural Environment Research Council (NE/N015479/1). Yang was supported by the National Natural Science Foundation of China (41961134031). Edward Keller, Martin Stokes, and an anonymous reviewer provided valuable comments and suggestions that helped improve the paper substantially.

Figures

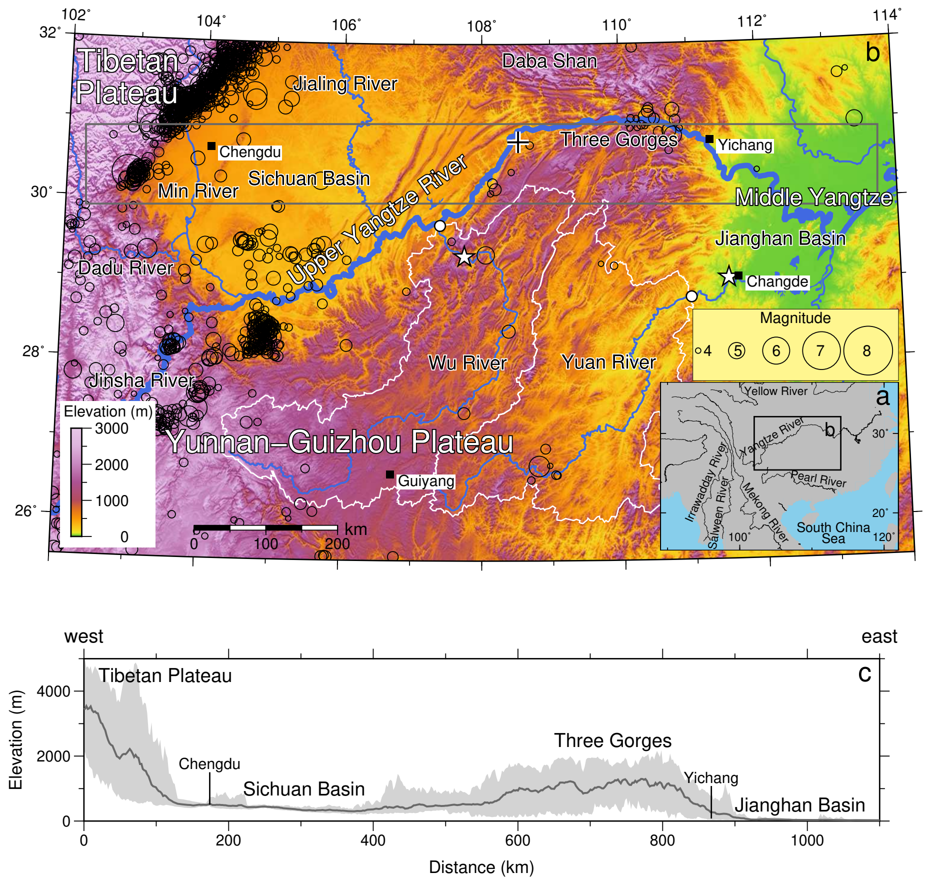

Figure 1: (a) Simplified map showing the major rivers of East Asia. (b) Topographic map (data from the GEBCO_2014 Grid) of the eastern Sichuan Basin and adjacent areas. Blue lines depict the main course (thick) and major tributaries (thin) of the Yangtze River. White lines depict the catchment boundaries of the Wu and Yuan Rivers. Open circles depict locations of earthquakes with magnitudes >4 between January 2000 and June 2021 (ANSS Comprehensive Earthquake Catalog). White dots depict the outlets of the two rivers to the Sichuan and Jianghan Basins, respectively. Plus and star symbols indicate sample locations of the apatite thermochronology (Shi et al., 2016) and cosmogenic ^{10}Be (Huang et al., 2013) data, respectively. Gray rectangle indicates location of the topographic swath profile in c. (c) Topographic swath profile across the Sichuan Basin. Gray shade shows surface elevations in the region projected onto the profile, whereas solid line depicts the mean elevations.

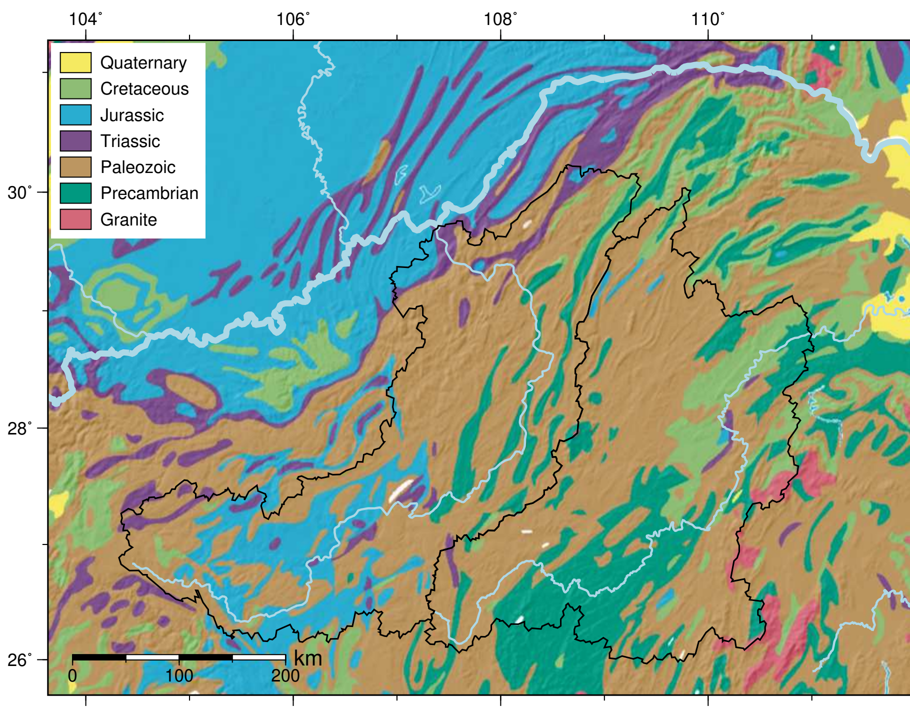

Figure 2: Simplified geological map of the study area, modified from the 1:5,000,000 Geological Map of China. Precambrian to Paleozoic units comprise mainly dolostone, siltstone, shale, pelite, and limestone; Triassic units comprise mainly sandstone, shale, limestone, and gypsum deposits; Jurassic and Cretacesou units comprise mainly sandstone and conglomerates; granites are of Mesozoic and Paleozoic ages (Yan et al., 2003). Blue lines depict the main course (thick) and major tributaries (thin) of the Yangtze River. Black lines depict the catchment boundaries of the Wu and Yuan Rivers.

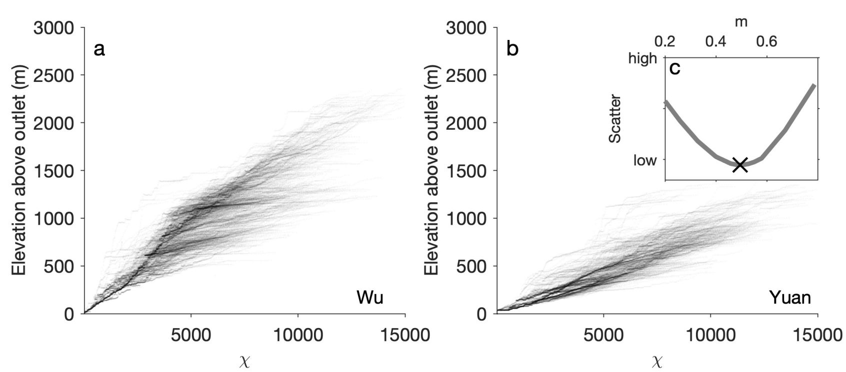

Figure 3: χ plots of the long profiles of the (a) Wu and (b) Yuan Rivers, calculated using Equations 3 and 5 with A_0=10^6 m^2 and m=0.50. (c) Scatter of the χ-plots using different values of m. Scatter is measured as the mean squared error of elevations at the same χ.

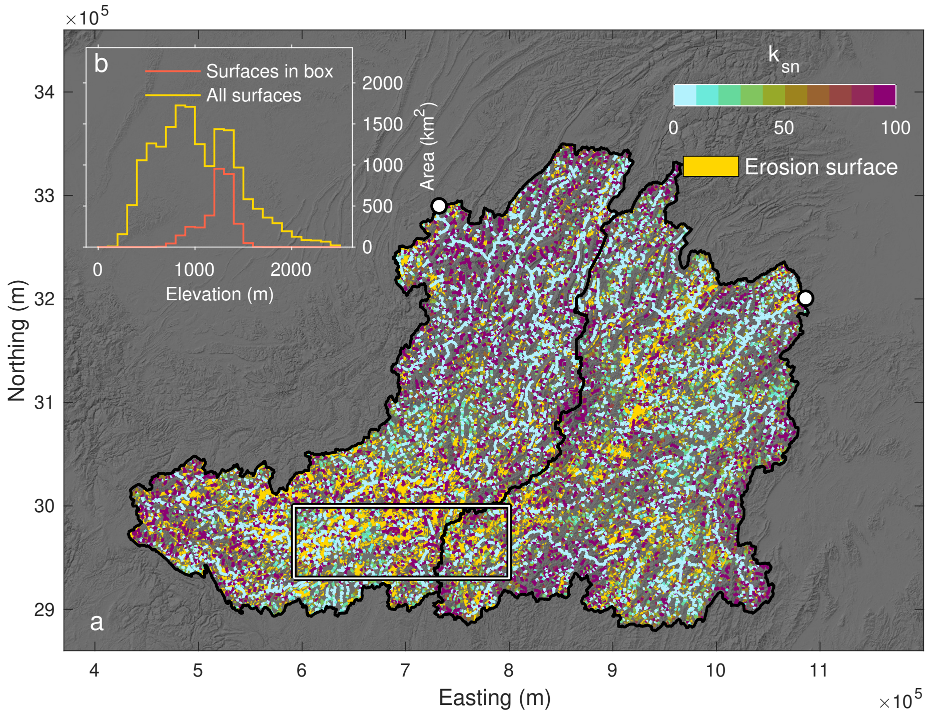

Figure 4: (a) Channel steepness and erosion surfaces mapped in the catchment areas of the Wu and Yuan Rivers. Yellow patches show erosion surfaces with areas >1 km^2. Mean elevations of the erosion surfaces of the two rivers in the boxed area are used as references for estimating the rivers' incision magnitudes (Figures 6 and 8). (b) Distributions of elevations of the erosion surfaces mapped within the catchment areas of the two rivers (yellow) and within the boxed area (red).

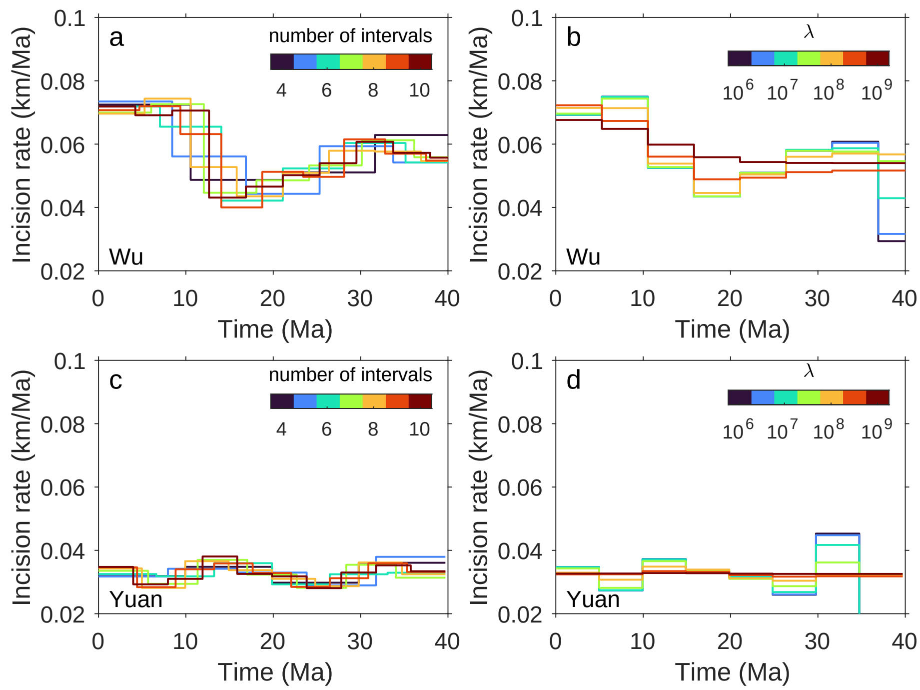

Figure 5: Models of the Wu and Yuan Rivers showing incision histories at their outlets in the Sichuan and Jianghan Basins, respectively. The model period is divided into a limited number of intervals with the same time (χ) span; during each interval a constant, spatially uniform uplift/incision rate is assumed. Modeled time and rates are calibrated using erosional efficiency $K = 4.03\times10^{-7}$ yr^{-1}, which is estimated using cosmogenic ^{10}Be derived basin-averaged erosion rates (Huang et al., 2013). (a and c) Models using a damping factor (λ) of $10^{7.5}$ and time interval numbers between 4 and 10. (b and d) Models using eight time intervals and damping factors between 10^6 and 10^9.

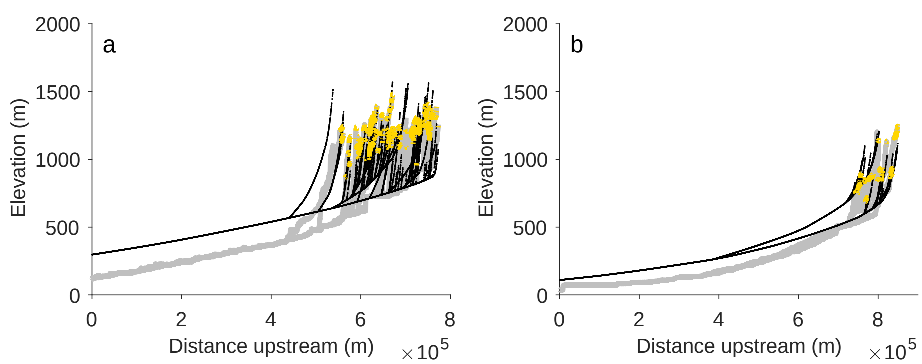

Figure 6: Long profiles of river channels with origins on the erosion surfaces in the boxed area shown in Figure 4a. Gray and black lines represent the present-day and reconstructed topography at the beginning of the model, respectively; channel topography is reconstructed by assuming a steady state between uplift and erosion. Yellow patches indicate channels on the erosion surfaces, where stationary elevation is assumed.

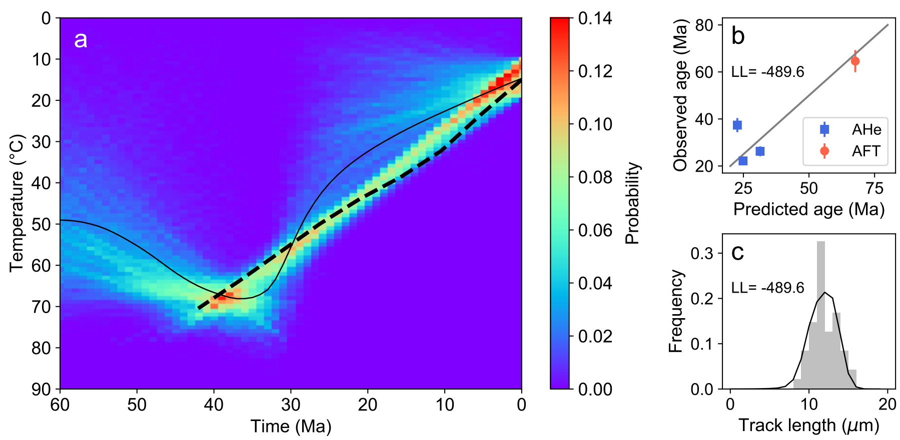

Figure 7: (a) Thermal history model of the eastern Sichuan Basin inverted using apatite fission-track (AFT) and (U-Th)/He (AHe) data from Shi et al. (2016). Color indicates the probability of the time-temperature points on the sampled cooling paths in the post-burn-in ensemble of the MCMC. Solid line depicts the mean model in the ensemble. Dashed line depicts the rock cooling path at the outlet of the Wu River to the Upper Yangtze, inferred based on the river's incision model (Figure 5a) with an erosional efficiency $K = 4.03\times10^{-7}$ yr^{-1} and a geothermal gradient of 22.5°C/km (Xu et al., 2011). (b) Observed AFT and AHe grain ages versus predictions by the mean model. Log-likelihood (LL) of the mean model is -489.6, with 99% of the post-burn-in models yield stable LL between -495.1 and 283.8. (c) Observed distribution of the AFT lengths (histogram) versus prediction by the mean model (curve).

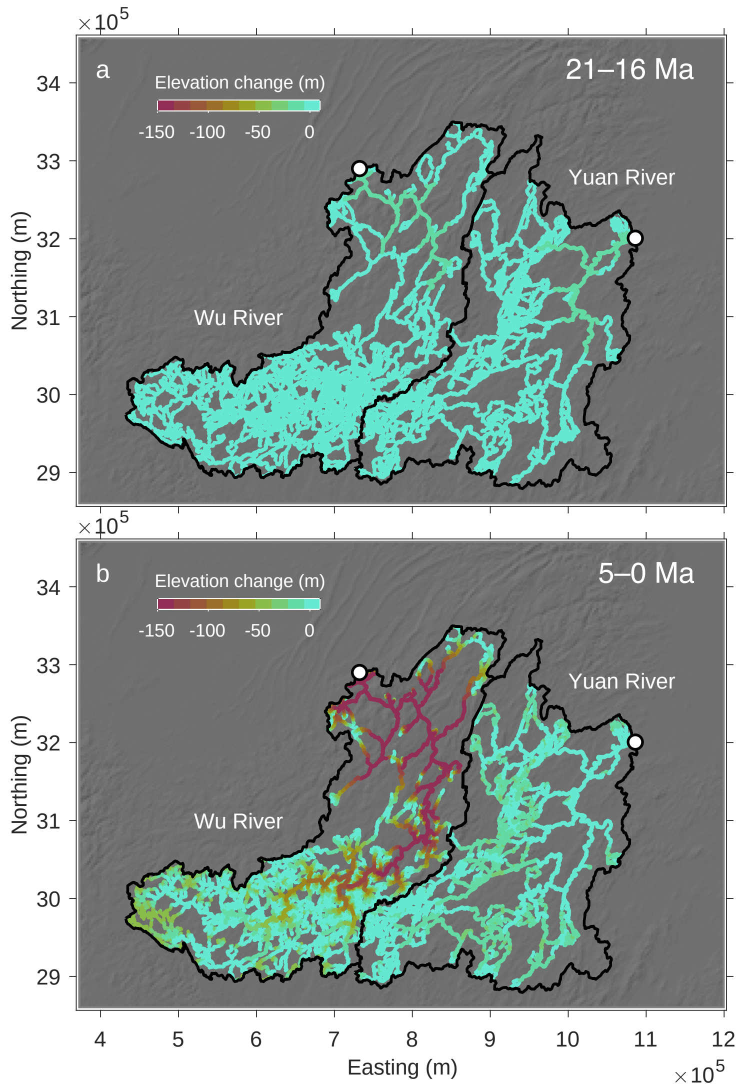

Figure 8: Inferred elevation changes of channels in the Wu and Yuan Rivers during (a) 21–16 Ma and (b) 5–0 Ma time intervals. Model uses eight time intervals and a damping factor (λ) of $10^{7.5}$. Elevation change is calculated relative to the assumed stable elevations of the erosion surfaces in an area across the drainage divide between the Wu and Yuan Rivers (boxed area in Figure 4a).

References

von Blanckenburg, F., 2005. The control mechanisms of erosion and weathering at basin scale from cosmogenic nuclides in river sediment. Earth and Planetary Science Letters 237, 462–479. doi:10.1016/j.epsl.2005.06.030.

Burchfiel, B.C., Chen, Z., Liu, Y., Royden, L.H., 1995. Tectonics of the Longmen Shan and Adjacent Regions, Central China. International Geology Review 37, 661–735. doi:10.1080/00206819509465424.

Cawood, P.A., Zhao, G., Yao, J., Wang, W., Xu, Y., Wang, Y., 2018. Reconstructing South China in Phanerozoic and Precambrian supercontinents. Earth-Science Reviews 186, 173–194. doi:10.1016/j.earscirev.2017.06.001.

Chappell, J., Zheng, H., Fifield, K., 2006. Yangtse River sediments and erosion rates from source to sink traced with cosmogenic 10Be: Sediments from major rivers. Palaeogeography, Palaeoclimatology, Palaeoecology 241, 79–94. doi:10.1016/j.palaeo.2006.06.010.

Chu, Y., Faure, M., Lin, W., Wang, Q., 2012. Early Mesozoic tectonics of the South China block: Insights from the Xuefengshan intracontinental orogen. Journal of Asian Earth Sciences 61, 199–220. doi:10.1016/j.jseaes.2012.09.029.

Clark, M.K., Royden, L.H., Whipple, K.X., Burchfiel, B.C., Zhang, X., Tang, W., 2006. Use of a regional, relict landscape to measure vertical deformation of the eastern Tibetan Plateau. Journal of Geophysical Research: Earth Surface 111, F03002. doi:10.1029/2005JF000294.

Clark, M.K., Schoenbohm, L.M., Royden, L.H., Whipple, K.X., Burchfiel, B.C., Zhang, X., Tang, W., Wang, E., Chen, L., 2004. Surface uplift, tectonics, and erosion of eastern Tibet from large-scale drainage patterns. Tectonics 23, 1–21. doi:10.1029/2002TC001402.

Dong, H., Wei, W., Jin, S., Ye, G., Zhang, L., Jing, J., Yin, Y., Xie, C., Jones, A.G., 2016. Extensional extrusion: Insights into south-eastward expansion of Tibetan Plateau from magnetotelluric array data. Earth and Planetary Science Letters 454, 78–85. doi:10.1016/j.epsl.2016.07.043.

Farley, K.A., 2000. Helium diffusion from apatite: General behavior as illustrated by Durango fluorapatite. Journal of Geophysical Research: Solid Earth 105, 2903–2914. doi:10.1029/1999JB900348.

Flint, J.J., 1974. Stream gradient as a function of order, magnitude, and discharge. Water Resources Research 10, 969–973. doi:10.1029/WR010i005p00969.

Fox, M., Carter, A., Dai, J.G., 2020. How Continuous Are the "Relict" Landscapes of Southeastern Tibet? Frontiers in Earth Science 8, 522. doi:10.3389/feart.2020.587597.

Fox, M., Goren, L., May, D.A., Willett, S.D., 2014. Inversion of fluvial channels for paleorock uplift rates in Taiwan. Journal of Geophysical Research: Earth Surface 119, 1853–1875. doi:10.1002/2014JF003196.

Gallagher, K., 2012. Transdimensional inverse thermal history modeling for quantitative thermochronology. Journal of Geophysical Research: Solid Earth 117, B02408. doi:10.1029/2011JB008825.

Garzanti, E., Andò, S., Vezzoli, G., 2008. Settling equivalence of detrital minerals and grain-size dependence of sediment composition. Earth and Planetary Science Letters 273, 138–151. doi:10.1016/j.epsl.2008.06.020.

Gleadow, A.J., Duddy, I.R., 1981. A natural long-term track annealing experiment for apatite. Nuclear Tracks 5, 169–174. doi:10.1016/0191-278X(81)90039-1.

Goren, L., Fox, M., Willett, S.D., 2014. Tectonics from fluvial topography using formal linear inversion: Theory and applications to the Inyo Mountains, California. Journal of Geophysical Research: Earth Surface 119, 1651–1681. doi:10.1002/2014JF003079.

Gourbet, L., Yang, R., Fellin, M.G., Paquette, J.L., Willett, S.D., Gong, J., Maden, C., 2020. Evolution of the Yangtze River network, southeastern Tibet: Insights from thermochronology and sedimentology. Lithosphere 12, 3–18. doi:10.1130/L1104.1.

Hack, J., 1957. Studies of longitudinal stream profiles in Virginia and Maryland. USGS Professional Paper 249 .

Haider, V.L., Kropáček, J., Dunkl, I., Wagner, B., von Eynatten, H., 2015. Identification of peneplains by multi-parameter assessment of digital elevation models. Earth Surface Processes and Landforms 40, 1477–1492. doi:10.1002/esp.3729.

Harrison, T.M., Copeland, P., Kidd, W.S.F., Yin, A., 1992. Raising Tibet. Science 255, 1663–1670. doi:10.1126/science.255.5052.1663.

Howard, A.D., Kerby, G., 1983. Channel changes in badlands. Geological Society of America Bulletin 94, 739–752. doi:10.1130/0016-7606(1983)94<739:CCIB>2.0.CO;2.

Huang, X., Zheng, H., Chappell, J., Wang, P., 2013. Characteristics of cosmogenic nuclide 10Be in the Yangtze riverine sediments and estimations of erosion rates (in Chinese with English abstract). Quaternary Sciences 33, 671–683. doi:0.3969/j.issn.1001-7410.2013.04.05.

Jiao, R., Yang, R., Yuan, X., 2021. Incision History of the Three Gorges, Yangtze River Constrained From Inversion of River Profiles and Low-Temperature Thermochronological Data. Journal of Geophysical Research: Earth Surface 126. doi:10.1029/2020JF005767.

Ketcham, R.A., 2005. Forward and Inverse Modeling of Low-Temperature Thermochronometry Data. Reviews in Mineralogy and Geochemistry 58, 275–314. doi:10.2138/rmg.2005.58.11.

Komar, P.D., 2007. Chapter 1 The Entrainment, Transport and Sorting of Heavy Minerals by Waves and Currents, in: Mange, M.A., Wright, D.T. (Eds.), Heavy Minerals in Use. Elsevier. volume 58 of *Developments in Sedimentology*, pp. 3–48. doi:10.1016/S0070-4571(07)58001-5.

Kong, P., Granger, D., Wu, F., Caffee, M., Wang, Y., Zhao, X., Zheng, Y., 2009. Cosmogenic nuclide burial ages and provenance of the Xigeda paleo-lake: Implications for evolution of the Middle Yangtze River. Earth and Planetary Science Letters 278, 131–141. doi:10.1016/j.epsl.2008.12.003.

Kong, P., Zheng, Y., Caffee, M.W., 2012. Provenance and time constraints on the formation of the first bend of the Yangtze River. Geochemistry, Geophysics, Geosystems 13, Q06017. doi:10.1029/2012GC004140.

Lee, J.S., Chao, Y., 1924. Geology of the gorge district of the Yangtze (from Ichang to Tzekuei) with special reference to the development of the gorges. Bulletin of the Geological Society of China 3, 351–392. doi:10.1111/j.1755-6724.1924.mp33-4004.x.

Lehner, B., Verdin, K., Jarvis, A., 2008. New Global Hydrography Derived From Spaceborne Elevation Data. Eos, Transactions American Geophysical Union 89, 93–94. doi:10.1029/2008EO100001.

Li, J., Xie, S., Kuang, M., 2001. Geomorphic evolution of the Yangtze Gorges and the time of their formation. Geomorphology 41, 125–135. doi:10.1016/S0169-555X(01)00110-6.

Li, S., Santosh, M., Zhao, G., Zhang, G., Jin, C., 2012. Intracontinental deformation in a frontier of super-convergence: A perspective on the tectonic milieu of the South China Block. Journal of Asian Earth Sciences 49, 313–329. doi:10.1016/j.jseaes.2011.07.026.

Liu, F., Gao, H., Pan, B., Li, Z., Su, H., 2019. Quantitative analysis of planation surfaces of the upper Yangtze River in the Sichuan-Yunnan Region, Southwest China. Frontiers of Earth Science 13, 55–74. doi:10.1007/s11707-018-0707-y.

Lv, L., Wang, L., Li, C., Li, H., Wang, X., Wang, S., 2020. Formation Mechanism for Upland Low-Relief Surface Landscapes in the Three Gorges Region, China. Remote Sensing 12, 3899. doi:10.3390/rs12233899.

Ma, Z., Zhang, H., Wang, Y., Tao, Y., Li, X., 2020. Inversion of Dadu River Bedrock Channels for the Late Cenozoic Uplift History of the Eastern Tibetan Plateau. Geophysical Research Letters 47. doi:10.1029/2019gl086882.

Malusà, M.G., Resentini, A., Garzanti, E., 2016. Hydraulic sorting and mineral fertility bias in detrital geochronology. Gondwana Research 31, 1–19. doi:10.1016/j.gr.2015.09.002.

Mcbride, E.F., 1985. Diagenetic Processes That Affect Provenance Determinations in Sandstone, in: Zuffa, G.G. (Ed.), Provenance of Arenites. Springer Netherlands, Dordrecht, pp. 95–113. doi:10.1007/978-94-017-2809-6_5.

Molnar, P., England, P., Martinod, J., 1993. Mantle dynamics, uplift of the Tibetan Plateau, and the Indian Monsoon. Reviews of Geophysics 31, 357—-396. doi:10.1029/93RG02030.

Nesbitt, H.W., Young, G.M., McLennan, S.M., Keays, R.R., 1996. Effects of Chemical Weathering and Sorting on the Petrogenesis of Siliciclastic Sediments, with Implications for Provenance Studies. The Journal of Geology 104, 525–542. doi:10.1086/629850.

Niemi, N.A., Oskin, M., Burbank, D.W., Heimsath, A.M., Gabet, E.J., 2005. Effects of bedrock landslides on cosmogenically determined erosion rates. Earth and Planetary Science Letters 237, 480–498. doi:10.1016/j.epsl.2005.07.009.

Perron, J.T., Royden, L., 2013. An integral approach to bedrock river profile analysis. Earth Surface Processes and Landforms 38, 570–576. doi:10.1002/esp.3302.

Pritchard, D., Roberts, G.G., White, N.J., Richardson, C.N., 2009. Uplift histories from river profiles. Geophysical Research Letters 36, 1–5. doi:10.1029/2009GL040928.

Qiu, L., Yan, D.P., Tang, S.L., Chen, F., Gong, L.X., Zhang, Y.X., 2020. Cenozoic exhumation of the Neoproterozoic Sanfang batholith in South China. Journal of the Geological Society 177, 412–423. doi:10.1144/jgs2019-041.

Reid, I.a.n., Frostick, L.E., 1985. Role of settling, entrainment and dispersive equivalence and of interstice trapping in placer formation. Journal of the Geological Society 142, 739–746. doi:10.1144/gsjgs.142.5.0739.

Richardson, N.J., Densmore, A.L., Seward, D., Fowler, A., Wipf, M., Ellis, M.A., Yong, L., Zhang, Y., 2008. Extraordinary denudation in the Sichuan Basin: Insights from low-temperature thermochronology adjacent to the eastern margin of the Tibetan Plateau. Journal of Geophysical Research 113, B04409. doi:10.1029/2006JB004739.

Richardson, N.J., Densmore, A.L., Seward, D., Wipf, M., Yong, L., 2010. Did incision of the Three Gorges begin in the Eocene? Geology 38, 551–554. doi:10.1130/G30527.1.

Riley, S., DeGloria, S.D., Elliot, R., 1999. A terrain ruggedness index that quantifies topographic heterogeneity. Intermountain Journal of Sciences 5, 23–27.

Roberts, G.G., Paul, J.D., White, N., Winterbourne, J., 2012. Temporal and spatial evolution of dynamic support from river profiles: A framework for Madagascar. Geochemistry, Geophysics, Geosystems 13, Q04004. doi:10.1029/2012GC004040.

Roberts, G.G., White, N., 2010. Estimating uplift rate histories from river profiles using African examples. Journal of Geophysical Research: Solid Earth 115, 1–24. doi:10.1029/2009JB006692.

Rosenbloom, N.A., Anderson, R.S., 1994. Hillslope and channel evolution in a marine terraced landscape, Santa Cruz, California. Journal of Geophysical Research: Solid Earth 99, 14013–14029. doi:10.1029/94JB00048.

Royden, L., Perron, J.T., 2013. Solutions of the stream power equation and application to the evolution of river longitudinal profiles. Journal of Geophysical Research: Earth Surface 118, 497–518. doi:10.1002/jgrf.20031.

Royden, L.H., Burchfiel, B.C., van der Hilst, R.D., 2008. The geological evolution of the Tibetan Plateau. Science 321, 1054–1058. doi:10.1126/science.1155371.

Rudge, J.F., Roberts, G.G., White, N.J., Richardson, C.N., 2015. Uplift histories of Africa and Australia from linear inverse modeling of drainage inventories. Journal of Geophysical Research: Earth Surface 120, 894–914. doi:10.1002/2014JF003297.

Rui, X., Stamps, D.S., 2019. A geodetic strain rate and tectonic velocity model for China. Geochemistry, Geophysics, Geosystems 20, 1280–1297. doi:10.1029/2018GC007806.

Schoenbohm, L., Whipple, K., Burchfiel, B., Chen, L., 2004. Geomorphic constraints on surface uplift, exhumation, and plateau growth in the Red River region, Yunnan Province, China. Geological Society of America Bulletin 116, 895—909. doi:10.1130/B25364.1.

Schwanghart, W., Scherler, D., 2014. Short Communication: TopoToolbox 2 - MATLAB-based software for topographic analysis and modeling in Earth surface sciences. Earth Surface Dynamics 2, 1–7. doi:10.5194/esurf-2-1-2014.

Shi, H., Shi, X., Glasmacher, U.A., Yang, X., Stockli, D.F., 2016. The evolution of eastern Sichuan basin, Yangtze block since Cretaceous: Constraints from low temperature thermochronology. Journal of Asian Earth Sciences 116, 208–221. doi:10.1016/j.jseaes.2015.11.008.

Su, H., Dong, M., Hu, Z., 2019. Late Miocene birth of the Middle Jinsha River revealed by the fluvial incision rate. Global and Planetary Change 183, 103002. doi:10.1016/j.gloplacha.2019.103002.

Sun, X., Tian, Y., Kuiper, K., Li, C., Zhang, Z., Wijbrans, J., 2021. No Yangtze River Prior to the Late Miocene: Evidence From Detrital Muscovite and K-Feldspar ^{40}Ar/^{39}Ar Geochronology. Geophysical Research Letters 48, e2020GL089903. doi:10.1029/2020GL089903.

Tapponnier, P., Peltzer, G., Le Dain, A.Y., Armijo, R., Cobbold, P., 1982. Propagating extrusion tectonics in Asia: New insights from simple experiments with plasticine. Geology 10, 611—-616. doi:10.1130/0091-7613(1982)10<611:PETIAN>2.0.CO;2.

Tapponnier, P., Xu, Z., Roger, F., Meyer, B., Arnaud, N., Wittlinger, G., Yang, J., 2001. Oblique Stepwise Rise and Growth of the Tibet Plateau. Science 294, 1671–1677. doi:10.1126/science.105978.

Tian, Y., Kohn, B.P., Qiu, N., Yuan, Y., Hu, S., Gleadow, A.J.W., Zhang, P., 2018. Eocene to Miocene Out-of-Sequence Deformation in the Eastern Tibetan Plateau: Insights From Shortening Structures in the Sichuan Basin. Journal of Geophysical Research: Solid Earth 123, 1840–1855. doi:10.1002/2017JB015049.

Tremblay, M.M., Fox, M., Schmidt, J.L., Tripathy-Lang, A., Wielicki, M.M., Harrison, T.M., Zeitler, P.K., Shuster, D.L., 2015. Erosion in southern Tibet shut down at $\sim$10 Ma due to enhanced rock uplift within the Himalaya. Proceedings of the National Academy of Sciences 112, 12030–12035. doi:10.1073/pnas.1515652112.

Vezzoli, G., Garzanti, E., Limonta, M., Andò, S., Yang, S., 2016. Erosion patterns in the Changjiang (Yangtze River) catchment revealed by bulk-sample versus single-mineral provenance budgets. Geomorphology 261, 177–192. doi:10.1016/j.geomorph.2016.02.031.

Wang, C., Zhao, X., Liu, Z., Lippert, P.C., Graham, S.A., Coe, R.S., Yi, H., Zhu, L., Liu, S., Li, Y., 2008. Constraints on the early uplift history of the Tibetan Plateau. Proceedings of the National Academy of Sciences of the United States of America 105, 4987–4992. doi:10.1073/pnas.0703595105.

Wang, M., Shen, Z., 2020. Present-day crustal deformation of continental China derived from GPS and its tectonic implications. Journal of Geophysical Research: Solid Earth 125. doi:10.1029/2019JB018774.

Wang, P., 2004. Cenozoic Deformation and the History of Sea-Land Interactions in Asia, in: Clift, P., Kuhnt, W., Wang, P., Hayes, D. (Eds.), Continent-Ocean Interactions Within East Asian Marginal Seas. American Geophysical Union (AGU), pp. 1–22. doi:10.1029/149GM01.

Wang, P., Zheng, H., Liu, S., 2013a. Geomorphic constraints on Middle Yangtze River reversal in eastern Sichuan Basin, China. Journal of Asian Earth Sciences 69, 70–85. doi:10.1016/j.jseaes.2012.09.018.

Wang, Q., 2001. Present-Day Crustal Deformation in China Constrained by Global Positioning System Measurements. Science 294, 574–577. doi:10.1126/science.1063647.

Wang, W., Zhao, J.H., Zhou, M.F., Pandit, M.K., Zheng, J.P., 2018a. Depositional age, provenance characteristics and tectonic setting of the Meso- and Neoproterozoic sequences in SE Yangtze Block, China: Implications on Proterozoic supercontinent reconstructions. Precambrian Research 309, 231–247. doi:10.1016/j.precamres.2017.11.012.

Wang, Y., Fan, W., Zhang, G., Zhang, Y., 2013b. Phanerozoic tectonics of the South China Block: Key observations and controversies. Gondwana Research 23, 1273–1305. doi:10.1016/j.gr.2012.02.019.

Wang, Y., Zhang, J., Zhang, B., Zhao, H., 2018b. Cenozoic exhumation history of South China: A case study from the Xuefeng Mt. Range. Journal of Asian Earth Sciences 151, 173–189. doi:10.1016/j.jseaes.2017.10.039.

Wessel, P., Smith, W.H.F., Scharroo, R., Luis, J., Wobbe, F., 2013. Generic Mapping Tools: Improved Version Released. Eos, Transactions American Geophysical Union 94, 409–410. doi:10.1002/2013EO450001.

Whipple, K.X., DiBiase, R.A., Ouimet, W.B., Forte, A.M., 2017. Preservation or piracy: Diagnosing low-relief, high-elevation surface formation mechanisms. Geology 45, 91–94. doi:10.1130/G38490.1.

Whipple, K.X., Tucker, G.E., 1999. Dynamics of the stream-power river incision model: Implications for height limits of mountain ranges, landscape response timescales, and research needs. Journal of Geophysical Research: Solid Earth 104, 17661–17674. doi:10.1029/1999JB900120.

Xu, M., Zhu, C.Q., Tian, Y.T., Rao, S., Hu, S.B., 2011. Borehole Temperature Logging and Characteristics of Subsurface Temperature in the Sichuan Basin. Chinese Journal of Geophysics 54, 224–233. doi:10.1002/cjg2.1604.

Yan, D.P., Zhou, M.F., Song, H.L., Wang, X.W., Malpas, J., 2003. Origin and tectonic significance of a Mesozoic multi-layer over-thrust system within the Yangtze Block (South China). Tectonophysics 361, 239–254. doi:10.1016/S0040-1951(02)00646-7.

Yan, Y., Carter, A., Huang, C.Y., Chan, L.S., Hu, X.Q., Lan, Q., 2012. Constraints on Cenozoic regional drainage evolution of SW China from the provenance of the Jianchuan Basin. Geochemistry, Geophysics, Geosystems 13, Q03001. doi:10.1029/2011GC003803.

Yang, R., Willett, S.D., Goren, L., 2015. In situ low-relief landscape formation as a result of river network disruption. Nature 520, 526–529. doi:10.1038/nature14354.

Yanites, B.J., Tucker, G.E., Anderson, R.S., 2009. Numerical and analytical models of cosmogenic radionuclide dynamics in landslide-dominated drainage basins. Journal of Geophysical Research 114, F01007. doi:10.1029/2008JF001088.

Zhang, P.Z., Shen, Z., Wang, M., Gan, W., Bürgmann, R., Molnar, P., Wang, Q., Niu, Z., Sun, J., Wu, J., Hanrong, S., Xinzhao, Y., 2004. Continuous deformation of the Tibetan Plateau from global positioning system data. Geology 32, 809–812. doi:10.1130/G20554.1.

Zhang, Z., Daly, J.S., Li, C., Tyrrell, S., Sun, X., Badenszki, E., Li, Y., Zhang, D., Tian, Y., Yan, Y., 2021. Formation of the Three Gorges (Yangtze River) no earlier than 10 Ma. Earth-Science Reviews 216, 103601. doi:10.1016/j.earscirev.2021.103601.

Zhao, G., 2015. Jiangnan Orogen in South China: Developing from divergent double subduction. Gondwana Research 27, 1173–1180. doi:10.1016/j.gr.2014.09.004.

Zheng, C., Xu, C., Brix, M.R., Zhou, Z., 2019. Evolution and provenance of the Xuefeng intracontinental tectonic system in South China: Constraints from detrital zircon fission track thermochronology. Journal of Asian Earth Sciences 176, 264–273. doi:10.1016/j.jseaes.2019.02.012.

Zheng, H., 2015. Birth of the Yangtze River: Age and tectonic-geomorphic implications. National Science Review 2, 438–453. doi:10.1093/nsr/nwv063.

Zheng, H., Clift, P.D., Wang, P., Tada, R., Jia, J., He, M., Jourdan, F., 2013. Pre-Miocene birth of the Yangtze River. Proceedings of the National Academy of Sciences 110, 7556–7561. doi:10.1073/pnas.1216241110.

Zheng, H., Jia, D., Chen, J., Wang, P., 2011. Did incision of the Three Gorges begin in the Eocene? COMMENT. Geology 39, e244–e244. doi:10.1130/G31944C.1.